Modulation transfer function of antenna-coupled infrared detector arrays

Glenn D. Boreman, Aristide Dogariu, Christos Christodoulou, and Dale Kotter

Individual antenna-coupled IR bolometers have recently been demonstrated at wavelengths near 10 μm. If focal-plane arrays (FPA's) of antenna-coupled detectors can be fabricated, enhancement of IR-imager performance is possible. A first step in the design process is to analyze the image-quality potential of antenna-coupled, FPA-based imagers in terms of the modulation transfer function (MTF). The key step in our analysis is development of a cross-talk MTF that accounts for the electromagnetic coupling between adjacent antennas in the FPA. We find that electromagnetic cross talk will not be a significant image-quality factor in antenna-coupled IR FPA's. © 1996 Optical Society of America

Key words: Infrared detector, bolometer, antenna, focal-plane array, image quality, modulation transfer function.

1. Introduction

Planar lithographic antennas have found wide application in the far-IR and millimeter-wave portions of the spectrum.[1] A recent demonstration[2] of this approach at thermal-IR wavelengths showed that a Au-on-Si spiral antenna facilitated efficient coupling of radiation to a subwavelength-sized bolometer at a wavelength of 9.5 μm. Potential advantages of antenna-coupled detectors in IR focal-plane-array (IR FPA) systems include faster response speed, increased sensitivity, increased directivity, simultaneous multiwaveband operation, and electronically tunable spectral and polarization responses. Antenna-coupling techniques are applicable to both bolometers[2] and photon detectors.[3] Given the potential advantages, it is of interest to examine the effect of an antenna-coupled FPA on the image quality obtained by an IR-imager system. Note that the focal-plane configuration being considered is an array of independent antenna-coupled detectors rather than a phased-array antenna. The detection process does not depend on phase coherence between signals on adjacent pixels because each antenna feeds its own individual power detector.

2. Definition of Imager-System PSF's

We analyze imager-system performance by means of point-spread functions (PSF's) and their Fourier transforms, the modulation transfer functions (MTF's). Sampling PSF's, diffraction-limited optics PSF's, and pixel PSF's are the PSF components[4] that apply to all sampled-image systems. Their convolution provides a baseline system PSF for image-quality comparison. We ignore in this analysis other causes of image-quality degradation (e.g., optical aberrations and thermal cross talk[5]) in an FPA imager system, because their magnitudes can be controlled to some extent by details of the system engineering.

To assess the image-quality effect of electromagnetic cross talk across a range of potential application platforms, we compare the overall MTF of antenna-coupled and non-antenna-coupled–imager systems, assuming two typical sets of values for sampling and optics PSF's.

A scene imaged onto a sampling array has a random position with respect to the sampling-lattice sites. This yields[4] (on average) a sampling PSF that is a rectangle function with a full width equal to the sampling interval. We define the standard system to have a sampling interval of 5λ, where λ is the wavelength of the incident radiation. This yields sampling intervals of 50 μm for operation around 10 μm and 25 μm for operation around 5 μm, typical of actual IR-imager systems. The enhanced system is

G. D. Boreman, A. Dogariu, and C. Christodoulou are with the Department of Electrical Engineering, Center for Research and Education in Optics and Lasers, University of Central Florida, Orlando, Florida 32816. D. Kotter is with the Idaho National Engineering Laboratory, Lockheed-Martin Corporation, Idaho Falls, Idaho 83415.

Received 15 November 1995; revised manuscript received 8 April 1996.

0003-6935/96/316110-05$10.00/0

assumed to employ a factor-of-2 spatial oversampling[6] and thus achieves a sampling interval of 2.5λ, one-half of the actual detector-array spacing.

The standard system is defined to have a circular-aperture, diffraction-limited $f/2$ optical system. This yields a Bessel-function optics PSF with an 86%-encircled-energy spot diameter of approximately 5λ. The enhanced system operates at $f/1$ and yields a diffraction-limited spot size of approximately 2.5λ.

3. Calculation of Pixel PSF for an Antenna-Coupled Detector

The pixel PSF will be different for antenna-coupled detectors and non-antenna-coupled detectors. For non-antenna-coupled detectors, the pixel PSF is just the spatial responsivity of the detector element itself.[7] We take the dimension of the non-antenna-coupled detectors to be a rectangle function of full width 4.5λ, which, considering the focal-plane sampling interval of 5λ, gives a fill factor of 81%, again typical of IR-imager systems.

The pixel PSF for an antenna-coupled detector consists of two components convolved together: the spatial responsivity of the antenna and the electromagnetic cross talk between adjacent antennas (a function of in-plane separation distance and direction). We perform our calculations for a planar Au-on-Si spiral antenna, for which measured performance data[2] and an analytical model for the antenna pattern[8] have been published.

A. Spatial-Responsivity PSF

In the case of radiation from a lithographic spiral antenna, propagating current waves on opposite arms of the antenna have identical directions and phases (assuming that the arms are driven antiphase) at a locus of points defined by a circle[9–11] with a circumference equal to the free-space illumination wavelength, so that $2\pi r = \lambda$. This spatial-resonance behavior determines the (free-space) width of the antenna pattern, because the radiation from current waves at other locations on the antenna arms interfere destructively and thus do not contribute to the radiation pattern.

When used for reception, an identical antenna pattern is obtained (by reciprocity), and the radiation falling in the one-wavelength-circumference circular region will produce the majority of the detector response. We thus take the spatial-responsivity portion of the pixel PSF as a ringlike delta function[12] of λ/π diameter. This delta-function representation is an idealization, but the main feature of the spatial responsivity, from an image-quality point of view, is the diameter of the ring. The fact that the spatial-responsivity PSF is actually a finite-width annulus will not appreciably change the pixel PSF once the spatial-responsivity PSF is convolved with the cross-talk PSF. We also assume that the majority of the signal appearing on the bolometer is collected from the antenna and is not caused by radiation falling on the bolometer itself. Given the small coupling efficiency of a subwavelength-sized detector, this assumption should be satisfied in practice.

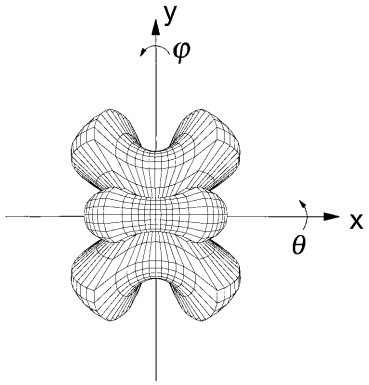

Fig. 1. Power radiation pattern of the dipole antenna as a function of θ and φ.

B. Electromagnetic-Cross-Talk PSF

The other component of the pixel PSF for an antenna-coupled detector is the electromagnetic cross talk, which is found by calculating the mutual impedance.[13] Conceptually, two antennas are located a distance s apart, and only the first antenna receives electromagnetic radiation. This radiation induces oscillating electric currents in the first. Without directly receiving the incoming radiation, the second antenna is excited by radiated electric fields produced by the currents in the first antenna. The strength of the signal received at the second antenna is proportional to the mutual impedance. Because the electric field of the first antenna falls off with distance, the mutual impedance tends to decrease with increasing separation.

We calculate the mutual impedance Z_{12}, using a method[14,15] based on the plane-wave spectrum of the far-field power radiation pattern of the antenna. This method is particularly convenient, because, although mutual impedance is a near-field phenomenon, the method in Refs. 14 and 15 requires only the far-field power radiation pattern to be known.

Using Eq. (73) of Ref. 15, we can write $Z_{12}(s/\lambda)$, the mutual impedance as a function of a normalized separation, as

$$Z_{12}(s/\lambda) = Z_0 \int_0^{2\pi} \int_{-j\infty}^{1} \exp[-j2\pi(s/\lambda)\cos\theta] \times P(\cos\theta, \varphi)\,\mathrm{d}\varphi\,\mathrm{d}(\cos\theta), \quad (1)$$

where P is the far-field power pattern of the antenna expressed as a function of cos θ and φ. The coordinates for Eq. (1) are consistent with Fig. 1 so that the in-plane separation s is in the y direction, angle φ is a rotation around the y axis, and angle θ is a rotation around the x axis.

Because lithographic antennas are illuminated from the dielectric side, we use the antenna pattern for a short dipole at a dielectric interface[16] for $P(\theta, \varphi)$ in Eq. (1). We recently obtained good agreement[8]

between this model and the measured data of Ref. 2 for spiral antennas at 9.5 μm. The power-radiation pattern[17] is a separable function of the orthogonal coordinates θ and φ, so that the product of the power patterns, P_θ and P_φ, inside the dielectric yields the radiation intensity (W sr^{-1}) at any compound angle:

$$P_\theta(\theta) = P_\theta(0)\left|\frac{n\cos[\sin^{-1}(n\sin\theta)]\cos\theta}{n\cos[\sin^{-1}(n\sin\theta)]+\cos\theta}\right|^2, \quad (2)$$

$$P_\varphi(\varphi) = P_\varphi(0)\left\{\frac{n\cos\varphi}{|\cos[\sin^{-1}(n\sin\varphi)]+n\cos\varphi|}\right\}^2. \quad (3)$$

We take the refractive index n of the dielectric as that of Si, equal to 3.4, and plot the product of P_θ and P_φ in Fig. 1. As required by Eq. (1), we express Eq. (2) in terms of $\cos\theta = t$ as

$$P_t(t) = P_t(1)\left|\frac{n\cos\{\sin^{-1}[n(1-t^2)^{1/2}]\}t}{n\cos\{\sin^{-1}[n(1-t^2)^{1/2}]+t}\right|^2 \quad (4)$$

and substitute Eqs. (3) and (4) into Eq. (1) to obtain

$$Z_{12}(s/\lambda) = Z_0\int_0^{2\pi} P(\varphi)\mathrm{d}\varphi\left\{\int_{-j\infty}^{0}\exp[-j2\pi(s/\lambda)t] \times P_t(t)\mathrm{d}t + \int_0^1 \exp[-j2\pi(s/\lambda)t]P_t(t)\mathrm{d}t\right\}. \quad (5)$$

The decrease of Z_{12} with separation s is the important quantity for our calculations rather than its absolute magnitude. We define Z_{12} only for $s \geq \lambda/2\pi$, that is, for separations greater than the radius of the responsive zone of the antenna. The next step in the calculation of the pixel PSF is the convolution of this mutual-impedance function with the ringlike delta function. The resulting pixel PSF is normalized to one at zero shift, so that the value of the normalization constant Z_0 used in Ref. 15 and Eq. (5) does not affect the results.

We numerically evaluate Eq. (5) as a function of the separation s along the y direction. This separation direction yields the minimum-cross-talk case. If the antenna pattern is rotated in-plane by 90 deg to exchange the variables θ and φ in Eqs. (2) and (3), the mutual-impedance magnitude function is found to be virtually identical. However, it is intuitive from Fig. 1 that the mutual impedance decreases more slowly with s in a direction corresponding to the maxima of the pattern. The dipole used to model the spiral has an in-plane rotation angle[16] that depends on both the illumination wavelength and the geometric layout of the antenna. We thus plot in Fig. 2 the antenna pattern from Fig. 1 along three different cuts: $\theta = 0$, $\varphi = 0$, and the diagonal cut corresponding to its maximum radial extent. To estimate the worst-case cross-talk performance for lithographic IR antennas, we empirically construct an angularly symmetric envelope function $P_e(\theta)$,

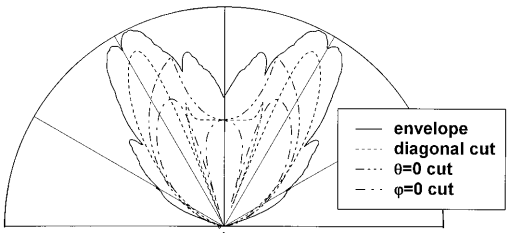

Fig. 2. Power radiation pattern of the dipole antenna along three cuts: $\theta = 0$, $\varphi = 0$, and a diagonal cut corresponding to the pattern's maximum radial extent. Also shown is the envelope function $P_e(\theta)$.

$$P_e(\theta) = 15(\cos 2\theta)^{1/2} + \sum_{m=0}^{10}\frac{2.4}{1.2^m} \times\left(\left\{\cos\left[6\left(\theta - \frac{\pi}{3+m}\right)\right]\right\}^{1/2} + \left\{\cos\left[6\left(\theta + \frac{\pi}{3+m}\right)\right]\right\}^{1/2}\right), \quad (6)$$

that encloses all three cuts, shown as the solid curve in Fig. 2. We use Eq. (6) in place of Eqs. (2) and (3) in the calculation of a worst-case $Z_{12}(s/\lambda)$.

C. Convolution of Pixel-PSF Components

Once the best-case and worst-case mutual-impedance functions are calculated, they are convolved with the ringlike delta function of diameter λ/π. In both cases, $Z_{12}(s/\lambda)$ was assumed to be circularly symmetric so that the two-dimensional convolution can be performed as a single integral.[18] When normalized to one at zero shift, these convolutions become the best-case and worst-case pixel PSF's for the antenna-coupled detector. They are shown in Fig. 3 along with the pixel PSF corresponding to the non-antenna-coupled detector. We show the corresponding pixel MTF's in Fig. 4 where the narrow core of the antenna-coupled pixel PSF substantially increased the pixel MTF at high frequencies compared with the non-

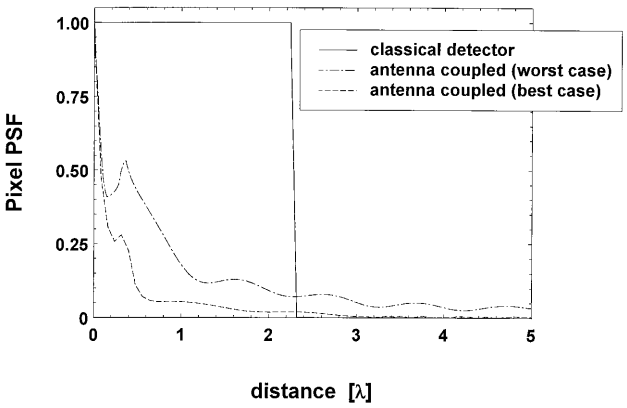

Fig. 3. Pixel PSF for a classical detector of full width 4.5λ along with best- and worst-case pixel PSF's for antenna-coupled detectors.

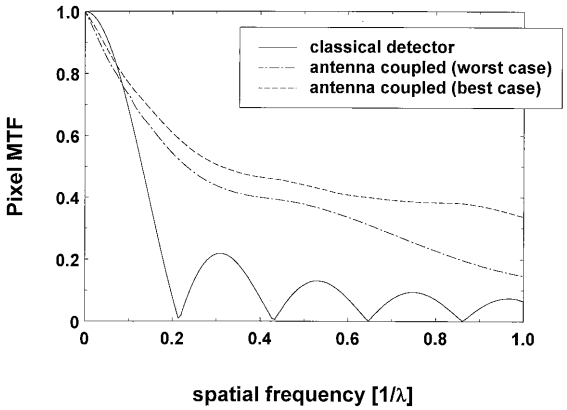

Fig. 4. Pixel MTF for a classical detector of full width 4.5λ along with best- and worst-case pixel MTF's for antenna-coupled detectors.

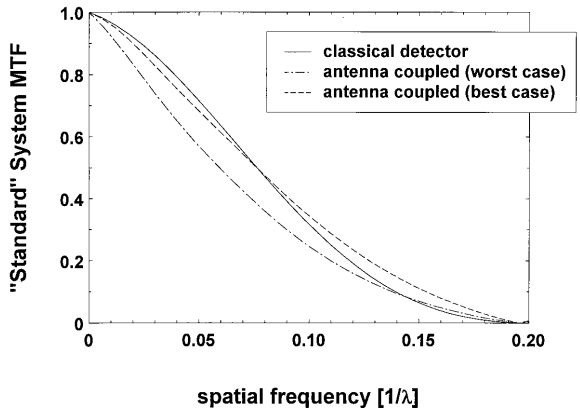

Fig. 5. System MTF's for a standard ($f/2$ optics and sample spacing of 5λ) system. Included in these system MTF's are the pixel MTF's seen in Fig. 4 for a classical detector of full width 4.5λ along with best- and worst-case pixel MTF's for antenna-coupled detectors.

antenna-coupled case. The effect of the extended interaction length, particularly in the worst case, is seen as a decreased pixel MTF at spatial frequencies lower than $0.1/\lambda$.

In the design of an antenna-coupled IR FPA, the in-plane rotation angle of the antennas should be adjusted with respect to the sampling lattice of the FPA to produce the condition that the closest neighboring pixels are in the directions with lowest cross talk and the (farther) diagonal neighbors are in a higher-cross-talk direction.

4. Comparison of Imager-System MTF Results

Whether the pixel MTF differences seen in Fig. 4 are important in a given imaging system depends on the other subsystem components, corresponding to a sampling MTF and an optics MTF. We compare two typical IR-imager-system configurations. A standard system with diffraction-limited $f/2$ optics and a 5-λ sampling interval will have an optics-MTF cutoff frequency at $0.5/\lambda$ and a sampling-MTF first-zero frequency at $0.2/\lambda$. An enhanced system with diffraction-limited $f/1$ optics and a 2.5-λ sampling interval will have an optics-MTF cutoff frequency at $1/\lambda$ and a sampling-MTF first-zero frequency at $0.4/\lambda$. When combined with the pixel MTF's of Fig. 4, we obtain the system MTF's shown in Fig. 5 for the standard system and in Fig. 6 for the enhanced system.

Referring to Fig. 5, we find that for the standard system, all configurations exhibit the $0.2/\lambda$ cutoff from sampling. The classical-detector case and the best antenna-coupled-detector case are virtually the same over the spatial-frequency range from 0 to $0.2/\lambda$. The worst antenna-coupled case has a maximum MTF penalty of 10% at midband compared with the classical-detector case.

In Fig. 6 for the enhanced system, the classical-detector case has a zero at $0.22/\lambda$ corresponding to the pixel dimension of 4.5 λ. The increase in the sampling MTF zero to $0.4/\lambda$ allows the better high-frequency MTF of the antenna-coupled detectors to raise the MTF above that of the classical-detector case. Around the classical-detector cutoff frequency, MTF gains of as much as 25% are possible in the best case, and MTF gains of as much as 15% are possible in the worst case. The maximum worst-case penalty is 15%, and the crossover frequency at which the MTF of the antenna-coupled system is better than the classical system is around $0.08/\lambda$ for the best case and $0.14/\lambda$ for the worst case.

5. Conclusions

Our results for both spatial responsivity and cross talk should be generally representative of the relatively low-gain lithographic-antenna designs currently under investigation for IR FPA applications. Although the spatial responsivity of an antenna depends on the particular antenna design (e.g., spiral, log-periodic, or bowtie), all lithographic antennas depend on similar spatial-resonance requirements between the wavelength and the antenna structure. Another similarity in the lithographic antennas is

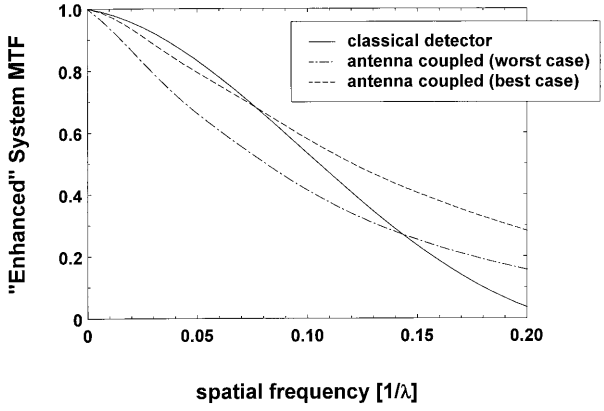

Fig. 6. System MTF's for an enhanced ($f/1$ optics and sample spacing of 2.5λ) system. Included in these system MTF's are the pixel MTF's seen in Fig. 4 for a classical detector of full width 4.5λ along with best- and worst-case pixel MTF's for antenna-coupled detectors.

that they are illuminated through their dielectric substrate. The refractive index of the dielectric will bound the angular width of the antenna pattern by means of Snell's law. Because the electromagnetic cross talk depends on the strength of the antenna pattern in any particular direction, most IR lithographic-antenna designs should have similar cross-talk characteristics. To make our cross-talk analysis more broadly applicable, we defined an angularly symmetric envelope function that completely encloses the antenna pattern used to model the spiral, and this envelope pattern was the basis for a worst-case analysis. If higher-gain antenna designs are used, the antenna patterns will be narrower and the cross talk consequently smaller.

Antenna-to-antenna cross talk causes a modest MTF decrease at low spatial frequencies, whereas the narrow spatial-responsivity PSF causes modest MTF gains at higher spatial frequencies. Systems that employ spatial oversampling and low-f/number optics are best able to capitalize on this high-frequency MTF enhancement. Overall we find that electromagnetic cross talk will not be a significant image-quality factor in antenna-coupled IR FPA's.

This research was supported in part by the U. S. Department of Energy under contract C95-175599-LKK-214-95.

References

1. D. Rutledge, D. Neikirk, and D. Kasilingham, "Integrated-circuit antennas," in *Infrared and Millimeter Waves*, K. J. Button, ed. (Academic, New York, 1983), Vol. 10, pp. 1–90.
2. E. Grossman, J. Sauvageau, and D. McDonald, "Lithographic spiral antennas at short wavelengths," Appl. Phys. Lett. **59,** 3225–3227 (1991).
3. C. Karadi, J. Jauhar, L. Kouwenhoven, K. Wald, J. Orenstein, P. McEuen, Y. Nagamune, and H. Sakaki, "Dynamic response of a quantum point contact," J. Opt. Soc. Am. B **11,** 2566–2571 (1994).
4. S. Park, R. Schowengerdt, and M. Kaczynski, "Modulation-transfer-function analysis for sampled image systems," Appl. Opt. **23,** 2572–2582 (1984).
5. E. Grossman, D. McDonald, and J. Sauvageau, "Two-dimensional analysis of microbolometer arrays," J. Appl. Phys. **68,** 5409–5414 (1990).
6. K. Barnard and E. Watson, "Effects of image noise on submicroscan interpolation," Opt. Eng. **34,** 3165–3173 (1995).
7. G. Boreman and A. Plogstedt, "Spatial filtering by a line-scanned nonrectangular detector—application to SPRITE readout MTF," Appl. Opt. **28,** 1165–1168 (1989).
8. G. Boreman, A. Dogariu, C. Christodoulou, and D. Kotter, "Dipole-on-dielectric model for infrared lithographic spiral antennas," Opt. Lett. **21,** 309–311 (1996).
9. J. Dyson, "The equiangular spiral antenna," IRE Trans. Antennas Propag. **7,** 181–187 (1959).
10. J. Kaiser, "The Archimedean two-wire spiral antenna," IRE Trans. Antennas Propag. **8,** 312–323 (1960).
11. H. Nakano, *Helical and Spiral Antennas* (Wiley, New York, 1987), p. 111.
12. J. Gaskill, *Linear Systems, Fourier Transforms, and Optics* (Wiley, New York, 1978), p. 77.
13. K. Lee, *Principles of Antenna Theory* (Wiley, New York, 1984), pp. 85–106.
14. G. Borgiotti, "A novel expression for the mutual admittance of planar radiating elements," IEEE Trans. Antennas Propag. **16,** 329–333 (1968).
15. W. Wasylkiwskyj and W. Kahn, "Theory of mutual coupling among minimum scattering antennas," IEEE Trans. Antennas Propag. **18,** 204–216 (1970).
16. C. Brewitt-Taylor, D. Gunton, and H. Rees, "Planar antennas on a dielectric surface," Electron. Lett. **17,** 729–731 (1981).
17. D. Rutledge and M. Muha, "Imaging antenna arrays," IEEE Trans. Antennas Propag. **30,** 535–537 (1982).
18. J. Gaskill, *Linear Systems, Fourier Transforms, and Optics* (Wiley, New York, 1978), p. 300.